

1 **Colloidal properties and stability of aqueous suspensions of few-layer graphene:**
2 **Importance of graphene concentration**

3 Yu Su ^a, Guoqing Yang ^a, Kun Lu ^a, Elijah J. Petersen ^b, Liang Mao ^{a,*}

4 ^a State Key Laboratory of Pollution Control and Resource Reuse, School of the Environment,
5 Nanjing University, Nanjing 210093, P. R. China;

6 ^b Material Measurement Laboratory, Biosystems and Biomaterials Division, National Institute of
7 Standards and Technology, 100 Bureau Drive, Stop 8311, Gaithersburg, MD 20899-0001, USA

8 *Corresponding author. Tel: +86 025-83594532. Email: lmao@nju.edu.cn (Liang Mao).

9
10
11
12
13
14
15
16
17
18
19
20
21

22 **ABSTRACT**

23 Understanding the colloidal stability of graphene is essential for predicting its transport and
24 ecological risks in aquatic environments. We investigated the agglomeration of ¹⁴C-labeled few-layer
25 graphene (FLG) at concentrations spanning nearly four orders of magnitude (2 μg/L to 10 mg/L) using
26 dynamic light scattering and sedimentation measurements. FLG agglomerates formed rapidly in
27 deionized water at concentrations > 3 mg/L. From 1 mg/L to 3 mg/L, salt-induced agglomeration was
28 decreased with dilution of FLG suspensions; the critical coagulation concentration of the more
29 concentrated suspension (3 mg/L) was significantly lower than the dilute suspension (1 mg/L) in the
30 presence of NaCl (1.6 mmol/L and 10 mmol/L, respectively). In contrast, FLG underwent slow
31 agglomeration and settling at concentrations ≤ 0.1 mg/L in NaCl solutions and ambient waters with
32 low ionic strength (< 10 mmol/L). Although salt-induced agglomeration led to 67 % reduction in
33 number of small FLG (25 nm to 50 nm) according to atomic force microscopy characterization,
34 transition from concentrated to dilute suspension retarded the removal of the small FLG. Additionally,
35 the small FLG exhibited greater bioaccumulation in zebrafish embryo and stronger chorion penetration
36 ability than larger ones. These findings suggest that FLG at more environmentally relevant
37 concentration is relatively stable and may have implications for exposure of small FLG to ecological
38 receptors.

39

40 **Keywords**

41 graphene; nanomaterial; agglomeration; sedimentation; bioaccumulation.

42

43

44

45

46 1. Introduction

47 Graphene, a new carbon-based nanomaterial (CNM), since first isolated by Novoselov et al. in
48 2004 (Novoselov et al., 2004), has attracted increasing attention because of its extraordinary properties
49 and potential applications (Geim, 2009; Novoselov et al., 2012), such as in composites (Ramanathan
50 et al., 2008; Stankovich et al., 2006), ultrasensitive sensors (Schedin et al., 2007), and transparent
51 conductive films (Eda et al., 2008; Wang et al., 2008). Currently, graphene is being incorporated into
52 a broad range of commercial products at a rapid rate (Segal, 2009). The increasing production and use
53 of graphene will inevitably lead to its release into the environment. Unfortunately, the environmental
54 behaviors of graphene are still largely unknown. To date, the majority of studies have focused on the
55 human health-related issues of graphene (Bussy et al., 2013; Duch et al., 2011; Schinwald et al., 2012;
56 Seabra et al., 2014; Yang et al., 2011; Yang et al., 2010; Zhang et al., 2010), with only a limited
57 number of studies on potential ecological risks (Guo et al., 2013; Hu et al., 2014; Hu et al., 2015). The
58 exposure of nanomaterials is directly determined by their transport and fate in the environment (Batley
59 et al., 2012; Lowry et al., 2012; Maurer-Jones et al., 2013). Once released into aquatic systems,
60 graphene is likely to interact with ubiquitous inorganic ions and natural organic matter (NOM).
61 Changes in graphene size and shape resulting from agglomeration may subsequently alter its mobility
62 as well as its reactivity and toxicity (e.g., to algal cells and wheat roots) (Hu et al., 2014; Hu et al.,
63 2015). Therefore, knowledge of the agglomeration behavior of graphene in aquatic environments is
64 essential for predicting its fate and potential for ecological exposure.

65 Agglomeration and stability of fullerene (nC_{60}) (Anderson and Barron, 2005; Bouchard et al., 2009;
66 Chen and Elimelech, 2006, 2008, 2009), carbon nanotube (CNT) (Sano et al., 2001; Smith et al., 2008;
67 Smith et al., 2009), and graphene oxide (GO) (Chowdhury et al., 2013; Chowdhury et al., 2015; Huang
68 et al., 2016; Konkana and Vasudevan, 2012; Wu et al., 2013) have been extensively studied in the
69 literature. These studies showed that the agglomeration of CNMs follows the Derjaguin-Landau-

70 Verwey-Overbeek (DLVO) theory, and the CNM-specific properties have strong effects on the
71 colloidal stability of CNMs. For example, the critical coagulation concentration (CCC) of cations was
72 found to increase with the increasing surface oxygen contents of CNT and GO (Chowdhury et al.,
73 2015; Smith et al., 2009; Yi and Chen, 2011). This suggests that pristine graphene with a hydrophobic
74 lattice may undergo layer-to-layer agglomeration in water at low ionic strength (IS). As mass
75 concentration affects particle number and the rate of collisions between colloids that have small
76 Hamaker constants and low surface potentials (Hsu and Liu, 1998), salt-induced agglomeration is
77 expected to be reduced at a low graphene concentration. However, no study has yet been conducted
78 to quantitatively establish the agglomeration kinetics of graphene as a function of electrolyte
79 concentration or to test the impact of mass concentration on its colloidal stability. In addition, for
80 graphene with nonuniform particle size distribution, agglomeration and settling cause increased
81 heterogeneity in water column (Petersen et al., 2015). It is likely that small graphene particles remain
82 suspended for longer time periods in dilute suspensions than the thicker ones. Characterization of size
83 distribution of the suspended CNMs is over-looked by the previous investigations. Moreover, it is very
84 important to evaluate the environmental risks of small graphene when ecological receptors tend to
85 ingest small nanomaterials (Mu et al., 2012; Silva et al., 2014; Zhao and Wang, 2012).

86 The objective of this paper is to ascertain the impact of mass concentration on agglomeration and
87 stability of ¹⁴C-labeled graphene, which mainly comprised four graphene layers (Guo et al., 2013) and
88 were defined as few-layer graphene (FLG) in our previous work (Feng et al., 2015; Lu et al., 2015;
89 Mao et al., 2016). The potential ecological risks of the suspended small FLG (S-FLG) were also
90 investigated. The agglomeration kinetics of FLG (0.1 mg/L to 10 mg/L) at varying IS were
91 investigated by using dynamic light scattering (DLS) method. To investigate the state of
92 agglomeration of FLG at concentrations (2 µg/L to 107 µg/L) that are below the detection limit of
93 DLS and most other analytical techniques, sedimentation kinetics in simple electrolyte solutions and

94 ambient water samples were performed via radioactivity measurements. While performing
95 experiments with varying compositions is necessary to yield a mechanistic understanding, it is critical
96 to verify that those trends are still observed in water samples from the natural and engineered
97 environment because some factors such as the type of NOM vary widely among water sources and the
98 NOM composition can impact the fate of environmental pollutants such as nanomaterials (Akkanen
99 et al., 2001; Pakarinen et al., 2013). After the size distribution of suspended FLG during the settling
100 experiments was characterized by atomic force microscopy (AFM), we prepared S-FLG by prolonged
101 sonication and evaluated if biological uptake of FLG by zebrafish (*Denio rerio*) embryo is size-
102 dependent.

103

104 **2. Materials and methods**

105 *2.1. Graphene synthesis and characterization*

106 Synthesis of ¹⁴C-labeled FLG by graphitization and exfoliation of sandwich-like
107 FePO₄/dodecylamine hybrid nanosheets has been described in our previous study (Guo et al., 2013).
108 Using X-ray photoelectron spectroscopy (XPS), the atomic ratio of C:O in the FLG was determined
109 to be 89:6 (the remaining 5 % is 1.4 % of H and 3.6 % of N) (Guo et al., 2013), and carbonyl (C=O),
110 hydroxyl (C-OH), and carboxyl (COOH) functional groups were found on the FLG surface (Feng et
111 al., 2015). Notably, the oxygen was introduced by the addition of ¹⁴C-phenol during the FLG synthesis,
112 not by oxidation. The specific radioactivity of FLG was determined to be (16.0 ± 0.6) mCi/g (n=3;
113 uncertainties always indicate standard deviation values if not specified). A stock suspension of FLG
114 (20 mg/L) was prepared following the procedures that are provided in the Supporting Information (SI),
115 and its radioactivity was determined via liquid scintillation counting (LSC) (LS 6500, Beckman
116 Coulter).

117

118 2.2. *Electrophoretic mobility measurements*

119 The electrophoretic mobility (EPM) of FLG (1 mg/L to 10 mg/L) was measured at varying NaCl
120 and NOM concentration at pH 7.0 and 25 °C using a disposable folded capillary cell (Nano ZS,
121 Malvern). Because the calculation of zeta potential values from EPM measurements uses the Henry
122 equation and the Smoluchowski approximation which assumes spherical particles, it is problematic to
123 use this approach for non-spherical CNMs (Petersen and Henry, 2012); EPM values are reported
124 instead. As described in the SI, Suwannee River NOM (SRNOM) (RO isolation, International Humic
125 Substances Society) was used as a model NOM and a stock solution of SRNOM was prepared, which
126 had a total organic carbon (TOC) content of (8.6 ± 0.1) mg/L ($n=3$). The background TOC content in
127 the DI water was around 0.3 mg/L. For each solution condition, six measurements were conducted for
128 each of three samples.

129

130 2.3. *Graphene agglomeration and sedimentation kinetics*

131 DLS (Nano ZS, Malvern) was used to measure the intensity-averaged hydrodynamic diameter
132 (D_h) of FLG as functions of time and NaCl concentration in the absence and presence of SRNOM. For
133 each agglomeration experiment, equal volumes (0.5 mL) of the diluted FLG stock suspension and
134 NaCl solution in the absence and presence of SRNOM were separately pipetted into a disposable
135 polystyrene cuvette to yield a specific FLG, electrolyte and/or SRNOM concentration. The capped
136 cuvette was then briefly vortexed, placed in the DLS instrument, and the measurements were started
137 immediately. The scattered light intensity was detected by a photodetector at a scattering angle of 90°,
138 the D_h was recorded every 10 s by autocorrelation function until D_h reached 1.5-fold of the initial D_h
139 or until 360 data points had been acquired (Chowdhury et al., 2013; Smith et al., 2008). All
140 agglomeration experiments were conducted in triplicate at pH 7.0, at which the FLG is stable at low
141 IS. Detailed equations and parameters for calculation attachment efficiency (α_a) and CCC values are

142 provided in the SI. The FLG concentration in the DLS measurements was quantified by radioactivity
143 measurements and ranged from 0.1 mg/L to 10 mg/L. However, FLG concentrations below 1 mg/L
144 did not provide a sufficient signal for accurate DLS measurements and were not included in further
145 analysis.

146 The long-term stability of FLG at low concentrations (2 $\mu\text{g/L}$ to 107 $\mu\text{g/L}$) were evaluated both
147 in well-controlled simple electrolyte solution and in natural or engineered aqueous systems. Eight
148 ambient waters were collected and characterized. Details for water sampling locations and water
149 analysis are provided in Table S1 and the SI. The sedimentation experiments were initiated by mixing
150 25 mL of NaCl solution (0 mmol/L to 500 mmol/L, pH=7.0) or each of the eight waters with the FLG
151 stock suspension in 40 mL amber glass vials (95 mm by 27.5 mm, CNW Technologies) with Teflon-
152 lined screw caps. The mixture was then vortexed for 10 s and was left undisturbed for up to 28 d at 25
153 $^{\circ}\text{C}$. The concentrations of suspended FLG in different treatments were monitored via radioactivity
154 measurements (detailed procedures are provided in the SI). Preliminary experiments showed that the
155 total volume of the mixture (1 mL to 40 mL) had insignificant influence on the sedimentation of FLG
156 (Fig. S1). Control measurements performed by adding the ^{14}C -labeled FLG to each of the water
157 samples, mixing them, and then immediately sampling the radioactivity using LSC did not indicate a
158 statistically significant matrix interference for any of the waters. All settling experiments were
159 conducted in triplicate to verify experimental reproducibility. To determine the particle size of the
160 suspended FLG, identical sedimentation experiments were performed by mixing the FLG stock with
161 10 mmol/L NaCl solution to yeild the initial FLG concentration of 1 mg/L. After settling for 7 d (a
162 long enough period to reach equilibrium), the upper layer suspensions (i.e., 1/5 of the total volume)
163 were deposited on mica plate, air dried and then analyzed by AFM. The size distribution of FLG
164 suspension at the beginning of sedimentation experiment was also characterized by AFM as control.

165

166 2.4. *Uptake experiments*

167 Zebrafish embryos were exposed to FLG suspensions to compare the potential ecological effects
168 of FLG differed in lateral size. Before the uptake experiments, prolonged sonication (up to 60 h) was
169 conducted to prepare S-FLG stock suspension using the same procedures as the stock FLG. Size
170 distribution and elemental composition of S-FLG were analyzed by AFM and XPS, respectively. Fish
171 embryo exposure experiment was conducted according to the OECD standard test protocol (OECD,
172 2013). Briefly, the FLG and S-FLG stock suspensions were diluted separately by clean water to yield
173 exposure concentration of $(75 \pm 1) \mu\text{g/L}$ ($n=3$). Zebrafish embryos at 2 h post fertilization were
174 distributed in 96-well plates (one embryo per well); each well contained 100 μL of FLG or S-FLG
175 suspension. After that, the embryos were cultured at $(26 \pm 1) ^\circ\text{C}$ for 12 h, 24 h, and 48 h. Triplicate
176 experiments ($n=100$ embryos/ treatment/ replicate) were conducted. At each time point, one hundred
177 embryos were removed, each embryo was washed three times with DI water. After this procedure,
178 FLG aggregates were not visible on the membranes of the embryos, and contributions from the
179 attached FLG to the total mass of FLG associated with the chorion are thus expected to be insignificant.
180 Following the DI water rinse step, chorion and yolk in each embryo was carefully separated using the
181 method described by Orlova et al. (2014). Once the chorion was pulled away, the yolk was able to
182 freely swim out from the chorion. The collected chorions (or yolks) ($n=100$) were pooled and
183 combusted using biological oxidation (OX-500, Zinser Analytic), and then the radioactivity was
184 analyzed using LSC (Mao et al., 2016).

185 Another group of embryos was exposed to the S-FLG suspensions using the same procedure
186 described above. At 48 h, the randomly selected embryos were removed and rinsed with 0.1 M
187 phosphate buffered saline (PBS) buffer. The yolks were taken out of the embryos, rinsed with PBS
188 buffer, and fixed with 3 % glutaraldehyde for 24 h, which was followed by a post-fixation step with
189 1.0 % osmium tetroxide for 1 h. After dehydration in a series of (50, 70, 80, 95, and 100) % ethanol,

190 the samples were embedded with propylene oxide and epoxy mixture. Ultra-thin sections (the
191 thickness of each section was about 50 nm to 60 nm) were placed on formvar-coated copper grids (300
192 mesh)(Kwon et al., 2015). The sections of the yolks were stained with uranyl acetate and lead citrate
193 and observed using a FEI Tecnai TF20 high resolution transmission electron microscope (HRTEM)
194 to verify the presence of S-FLG in the yolk.

195

196 2.5. *DLVO interaction energy between FLG-FLG*

197 According to the DLVO theory, the total interaction energy between particles can be defined as
198 the sum of the van der Waals (VDW) attraction and the electrostatic double layer (EDL) repulsion
199 (Elimelech, 1995). The FLG-FLG interaction energy profiles under different FLG and NaCl
200 concentrations were calculated assuming plate-plate geometry (Elimelech, 1995; Gregory, 1981).
201 Detailed equations and parameters are presented in the SI.

202

203 2.6. *Statistical analysis*

204 One-way ANOVA with Tukey's multiple comparison tests was used to determine the statistical
205 differences in sedimentation rate constants and D_h values of FLG among different solution chemistries
206 and to compare differences in FLG contents that accumulated by organisms. Statistical difference was
207 set at $p < 0.05$.

208

209 **3. Results and Discussion**

210 3.1. *Agglomeration of graphene at high concentrations*

211 Cuvettes containing various concentrations (1 mg/L to 10 mg/L) of FLG dispersed in DI water
212 are shown in Fig. 1a. Since all FLG suspensions were optically transparent, the DLS method was
213 successfully used for measurement changes in the D_h of FLG as a function of time. The D_h values of

214 FLG were relatively constant in DI water within 1 h at a concentration range of 1 mg/L to 3 mg/L,
215 whereas FLG agglomerated within a few minutes at concentrations above 3 mg/L (Fig. 1b). This
216 showed that the stability of FLG was much weaker than that of GO, which was stable in DI water at
217 much higher concentrations (10 mg/L to 40 mg/L) (Chowdhury et al., 2013; Wu et al., 2013). For the
218 dilute FLG suspensions (1 mg/L to 3 mg/L), the presence of Na⁺ (e.g., 10 mmol/L) induced the
219 formation of agglomerates (Fig. 1c). Notably, the agglomeration was faster with increasing FLG
220 concentration at the same IS. For instance, the initial agglomeration rate constant (k_a) (i.e., the initial
221 rate of increase in D_h from $D_{h,initial}$ to $1.5D_{h,initial}$ with time) (Bouchard et al., 2012; Chowdhury et al.,
222 2013; Holthoff et al., 1996) of 3 mg/L of FLG was (0.2300 ± 0.0003) nm/s in 1 mmol/L NaCl, which
223 was 2.1 and 3.8 times higher than that of 2.5 mg/L $((0.110 \pm 0.003)$ nm/s) and 1 mg/L $((0.060 \pm 0.001)$
224 nm/s) of FLG, respectively. In addition, the k_a measured under diffusion-limited conditions increased
225 proportionally with FLG concentration ($R^2=0.9870$) (Fig. S2). This suggests that a narrow FLG
226 concentration range had a strong impact on the agglomeration behaviors.

227 Plots of attachment efficiency (α_a) as a function of NaCl concentration exhibit two distinct regions:
228 a reaction-limited regime where α_a increases with IS at low IS, and a diffusion-limited regime in which
229 α_a is independent of IS at higher NaCl concentrations (Fig. 1d). This indicates that the agglomeration
230 of FLG is in general agreement with the DLVO theory (Chen and Elimelech, 2006; Chen et al., 2006).
231 The intersection between the extrapolations through the reaction- and diffusion-limited regimes
232 yielded CCC value (Chen and Elimelech, 2006; Elimelech, 1995). Unexpectedly, the CCC values were
233 greatly affected by the concentrations of FLG, which were determined to be (1.550 ± 0.001) mmol/L,
234 (5.18 ± 0.03) mmol/L, and (9.960 ± 0.004) mmol/L NaCl for 3 mg/L, 2.5 mg/L, and 1 mg/L of FLG,
235 respectively. Likely mechanisms for this finding are discussed in later sections. As summarized in
236 Table S2, these CCC values are much lower than the CCC values for C₆₀ (120 mmol/L to 260 mmol/L
237 NaCl) (Bouchard et al., 2009; Chen and Elimelech, 2006), CNTs (37 mmol/L to 210 mmol/L NaCl)

238 (Sano et al., 2001; Smith et al., 2008; Yi and Chen, 2011), and GO (44 mmol/L to 188 mmol/L NaCl)
239 (Chowdhury et al., 2013; Wu et al., 2013), indicating that the FLG is less stable. Since the surface
240 oxygen content of CNMs has a great influence on their CCC values (Smith et al., 2009; Yi and Chen,
241 2011), the poorer stability of FLG may be attributed to its lower oxygen content (6 %) (Guo et al.,
242 2013) than that of other CNMs, such as the oxidized CNTs (10.6 %) (Yi and Chen, 2011) and GO
243 (60 %) (Chowdhury et al., 2015). Difference in particle size may also play an important role, but it is
244 challenging to make direct comparisons among the nominal hydrodynamic diameter values of CNMs
245 given their variable shapes.

246

247 3.2. *Effects of mass concentration on attachment efficiency of graphene*

248 The effect of particle concentration on the stability of colloids has been the subject of a number
249 of studies (Hanus et al., 2001; Hsu and Liu, 1998; Tezak et al., 1951), but no study has yet focused on
250 the CNMs. Agglomeration studies clearly showed that the effects of Na⁺ on the FLG-FLG interaction
251 followed the prediction of the DLVO theory (Chen and Elimelech, 2006; Chen et al., 2006), but the
252 attachment efficiency was largely different in a narrow FLG concentration (i.e., 1 mg/L to 3 mg/L)
253 under reaction-limited conditions (e.g., 1 mmol/L NaCl). We assume that the disparity in attachment
254 efficiency among these FLG concentrations should be caused by the difference in total interaction
255 energy. Particle size and zeta potential are key parameters that control the total interaction energy of
256 colloids according to the DLVO theory (Elimelech, 1995; Gregory, 1981). Since the initial D_h values
257 of FLG under these concentrations were not significantly different ($p > 0.05$) (Table S3), the effects
258 of Na⁺ on charge screening may be greater at higher FLG concentrations. So that the VDW attraction
259 overweighs the EDL repulsion more readily, allowing the FLG sheets to approach closer.
260 Electrophoretic mobility measurements showed that the absolute values of EPM in NaCl solutions (0
261 mmol/L to 100 mmol/L) gradually decreased as the FLG concentration increased from 1 mg/L to 10

262 mg/L (Fig. S3). For example, from 1 mg/L to 3 mg/L, the absolute values of EPM decreased from (-
263 2.03 ± 0.05) $\times 10^{-8}$ m²/Vs to (-1.49 \pm 0.06) $\times 10^{-8}$ m²/Vs in 1 mmol/L NaCl. This concentration-
264 dependent trending in the EPM was observed for titanium dioxide, polyurethane, and hexadecane
265 particles (Kaszuba et al., 2010; Medrzycka, 1991). The mechanism by which concentration affects the
266 EPM of FLG is unclear, but it can be sure that obscuration of light transmission is negligible as the
267 intensity of scattered light being detected was still very high at FLG concentration of 10 mg/L. The
268 DLVO interaction energy profiles between FLG-FLG as functions of FLG and NaCl concentrations
269 are shown in Table S4 and Fig. S4. At a given FLG concentration, the DLVO calculations predict the
270 presence of deepened secondary energy minima at higher NaCl concentration (from 0.5 mmol/L to 10
271 mmol/L), thus resulting in greater particle collision and attachment as observed from the
272 agglomeration experiments. An increase in the FLG concentration (from 1 mg/L to 3 mg/L) led to
273 higher secondary energy minima at 5 mmol/L and 10 mmol/L NaCl, indicating that FLG particles
274 agglomerate more readily in the more concentrated suspensions as a result of the increased attractive
275 forces. This is helpful for explanation the observed faster agglomeration at 3 mg/L of FLG than that
276 for 2 mg/L and 1 mg/L of FLG at same IS.

277

278 3.3. Long-term stability of graphene at low concentrations

279 To test the stability of FLG at more environmentally relevant concentrations below the DLS
280 detection limit and for longer time periods (7 d to 28 d), sedimentation experiments were conducted
281 using lower FLG concentrations (107 μ g/L to 2 μ g/L). During the first 60 minutes, the concentrations
282 of FLG remained constant and were not significantly different ($p > 0.05$) in varying NaCl solutions (0
283 mmol/L to 1000 mmol/L) (Fig. S5). Thereafter, the settling profiles of the FLG (Fig. 2a) exhibited
284 exponential decays and were well fitted by a first-order model (detailed procedures and results are
285 shown in the SI and Table S5), a model which has also recently been applied to fit the sedimentation

286 kinetics of other nanomaterials (Brunelli et al., 2013; Markus et al., 2015). The sedimentation rate
287 constants (k_s) of FLG (107 $\mu\text{g/L}$) increased with greater IS at low NaCl concentrations (from $(0.68 \pm$
288 $0.08) \text{ d}^{-1}$ at 0 mmol/L to $(1.3 \pm 0.2) \text{ d}^{-1}$ at 10 mmol/L; uncertainties of k_s indicate standard error values),
289 but did not significantly increase ($p > 0.05$) when the NaCl concentration was higher than 10 mmol/L
290 (i.e., 10 mmol/L compared to 50 mmol/L or 500 mmol/L NaCl) (Fig. 2b). Similar effects of Na^+ on
291 the stability of FLG were also observed for FLG concentrations of 11 $\mu\text{g/L}$ and 2 $\mu\text{g/L}$. Therefore, the
292 agglomeration of FLG varied with IS also in a manner consistent with the DLVO theory under these
293 low FLG concentrations. It is worth noting that particle concentration had a greater effect on the
294 sedimentation than the IS. At a given NaCl concentration (i.e., 10 mmol/L), the k_s of 2 $\mu\text{g/L}$ of FLG
295 was a factor of 13.5 and 2.7 times smaller than that of FLG at higher concentrations of 107 $\mu\text{g/L}$ and
296 11 $\mu\text{g/L}$, respectively (Table S5). This result is also consistent with our earlier observations that the
297 agglomeration of FLG was faster at higher FLG concentrations (i.e., 3 mg/L compared to 2.5 mg/L or
298 1 mg/L) (Fig. 1c).

299 The sedimentation kinetics of FLG in eight ambient waters ($\text{pH} = 7.7 \pm 0.4$; details for water
300 characteristics are provided in Table S6) showed that water type had a notable influence on the stability
301 of FLG (Fig. 3a and b). Destabilization of FLG occurred quickly in the East China Sea water and the
302 influent and treated effluent from a wastewater treatment plant (WWTP); the concentrations of FLG
303 (50 $\mu\text{g/L}$) were sharply reduced by $\sim 71\%$, $\sim 43\%$, and $\sim 40\%$ within 1 d, respectively. In comparison,
304 the FLG underwent slow agglomeration in other five freshwaters and underground waters;
305 approximately 42% - 65% of FLG (50 $\mu\text{g/L}$) remained suspended after one week, the lowest
306 sedimentation was observed for the Qinghai Lake water for which more than 70% of FLG (4 $\mu\text{g/L}$)
307 remained in aqueous phase after 28 d. Since the insoluble fraction was removed by filtration with a
308 0.22 μm cellulose acetate membrane, sedimentation was mainly affected by the IS of the waters. Plots
309 of the k_s versus the total IS (i.e., the sum of the IS of F^- , Cl^- , NO_3^- , SO_4^{2-} , K^+ , Na^+ , Ca^{2+} , and Mg^{2+}) of

310 the waters are shown in Fig. S6c. The k_s values of FLG were constant under lower total IS (0.234
311 mmol/L to 4.79 mmol/L), but significantly increased ($p < 0.05$) when the total IS approached 10
312 mmol/L. The presence of NOM (2.1 mg TOC/L to 34 mg TOC/L) had a stabilizing effect on FLG in
313 the low IS freshwaters and ground waters. The FLG had a high affinity for SRNOM at 10 mmol/L
314 NaCl (details of adsorption experiments are provided in SI) (Fig. S6). Adsorption of NOM
315 macromolecules onto FLG resulted in steric and electrostatic repulsions (the EPM values of FLG were
316 more negative with addition of SRNOM compared to NaCl alone (Fig. S7a), which effectively
317 retarded the agglomeration and sedimentation of FLG in 10 mmol/L NaCl (Fig. S7b and 2c); the CCC
318 for NaCl was increased by 9.5 times from (9.960 ± 0.004) mmol/L to (95.00 ± 0.09) mmol/L with
319 addition of SRNOM (0.57 mg TOC/L) (Fig. 1d). The sedimentation of FLG in ambient waters also
320 showed a strong dependence on FLG concentration. At a lower FLG concentration (4 $\mu\text{g/L}$), the k_s
321 values of FLG in all water samples were reduced by 1.7 to 4.4 times compared to a higher FLG
322 concentration (50 $\mu\text{g/L}$) (Table S6).

323

324 3.4. *Size distribution of suspended graphene*

325 The long-term stability studies further verified that the mass concentration of FLG played an
326 important role in affecting salt-induced agglomeration and settling. At higher concentrations, settling
327 of a single particle is often impacted by other particles. The formation of agglomerates accelerates the
328 sedimentation of the colliding particles and reduces the number of primary particle and total particle.
329 For FLG suspensions with nonuniform size distribution, small FLG sheets often diffuse faster than the
330 larger ones according to the Stokes-Einstein equation (Cho et al., 2011). It is possible that
331 agglomeration resulting from collisions between small-small or small-larger FLG sheets will reduce
332 the number of small particles. To confirm this hypothesis, the lateral size of FLG (1 mg/L, in 10
333 mmol/L NaCl) before and after sedimentation for 7 d was characterized by AFM. As shown in Fig. 4a

334 and b, settling process did not significantly affect the thickness of FLG, which was measured to be
335 (0.34–4.17) nm and (0.33–3.22) nm at 0 d and 7 d, respectively; 71 % (0 d) or 69 % (7 d) of total count
336 was in the range of (0.5–1) nm. However, sedimentation led to significant reduction in the total particle
337 number of FLG and removal of larger FLG sheets. The width of size distribution of FLG was shortened
338 from (20–993) nm (0 d) to (22–569) nm (7 d), as 4.4 % of total counted FLG ranging from 575 nm to
339 975 nm had settled out of water. The AFM results confirmed that 18 % of total counted FLG was in
340 the range of (25–50) nm at the beginning of sedimentation experiment (0 d). After settling for 7 d, the
341 fraction of these small FLG in aqueous phase was decreased to 6 %. When the number of primary
342 particles decreases to a threshold at which the motion of a single particle is less likely affected by the
343 surrounding particles, the small and large FLG sheets may settle independently, the agglomeration and
344 settling of primary particles slow down. Thus, the normalized concentrations (i.e., C/C_0) of FLG were
345 relatively constant at same IS from 3 d to 7 d at concentration of 107 $\mu\text{g/L}$ (Fig. 2a). It is worth noting
346 that FLG will take longer time to achieve the same degree of agglomeration under more dilute
347 conditions (e.g., 11 $\mu\text{g/L}$ and 2 $\mu\text{g/L}$). In such cases, decreasing mass concentration leads to slow
348 removal and a longer persistence of the small FLG (i.e., 25 nm to 50 nm) in water column and higher
349 potential of exposure to aquatic organism.

350

351 3.5. *Size-dependent uptake of graphene by zebrafish embryo*

352 Size dependence of cellular uptake, cytotoxicity, and antimicrobial activity have been observed for
353 GO (Ma et al., 2015; Mu et al., 2012; Perreault et al., 2015). It is still not known whether uptake of
354 pristine graphene by ecological receptor is size dependent. To explore impact of lateral size on
355 biological uptake of FLG and to avoid interference from Na^+ , we prepared S-FLG by prolonged
356 sonication (up to 60 h). Prolonged sonication did not significantly change the elemental composition
357 of FLG (data not shown), but greatly increased the percentage of (25-50) nm FLG from 18 % to 88 %

358 on the basis of AFM results (Fig. S8). In addition, analysis of the extracts using LSC and gas
359 chromatography-mass spectrometry (GC-MS) did not show a significant increase in the radioactivity
360 or obvious chemical peaks in GC-MS chromatograms of the extracted solutions, indicating that
361 degradation products were not formed from the prolonged sonication processes of FLG. Uptake of
362 FLG and S-FLG by zebrafish embryos was further investigated. The distribution of FLG within the
363 zebrafish embryos varied with the lateral size (Fig. 5a). When exposed to FLG for 12 h-48 h, 85 % -
364 98 % of the total mass of the accumulated FLG (i.e., the sum of the FLG contents in the chorion and
365 the yolk) was in the chorion and few of them was detected in the yolk. In comparison, the contents of
366 S-FLG in the chorion were significantly enhanced by 3.7, 3.0, and 1.6 times at 12 h, 24 h, and 48 h,
367 respectively. Moreover, 16 % - 21 % of the total mass of the accumulated S-FLG passed the chorion
368 to the yolk. To confirm the presence of the S-FLG in the yolk, ultra-thin sections of the yolk were
369 observed through HRTEM (Fig.5b), which shows visible ordered graphite lattices with interlayer
370 distance of 0.342 nm that is equal to the reported interlayer distance of graphite (Deng et al., 2011).
371 Well-defined diffraction spots that represent the crystalline structure of graphene (Brown et al., 2014)
372 were also observed in the fourier transfer image of Fig. 5b. These observations demonstrated that
373 decrease in size greatly enhanced the membrane penetration ability of FLG. The microstructure of the
374 chorion may be a decisive factor affecting the transmembrane transport of FLG. Zebrafish chorion
375 consists of three layers that are pierced by cone-shaped pore canals, given the narrow diameter (500
376 nm to 700 nm) (Rawson et al., 2000), these pores may restrict the uptake of large particles that
377 presented in FLG suspension. As mentioned previously, large FLG with lateral size ranging from 575
378 nm to 975 nm accounted for 4.4 % of the total counted FLG sheets (Fig. 4c). Because the mass of FLG
379 particles is proportional to the square of diameter, a 500 nm particle would have a factor of 100 more
380 mass than a 50 nm particle (assuming similar thickness). Unlike S-FLG, the mass of the large particles
381 mainly contributed to the total mass of FLG. The limited bioaccessibility of these large particles

382 impeded the accumulation of FLG in the yolk. In addition, the S-FLG may have different
383 agglomeration behavior from FLG, the more slowly S-FLG agglomerated, the more small particles
384 would be taken up by embryos.

385

386 **4. Conclusion**

387 The agglomeration behavior of graphene will dictate its transport and fate in the environment.
388 Our results show that the concentration of FLG is a key factor in its agglomeration and stability in
389 aqueous media, but one that was often overlooked in previous studies. At a given IS, the agglomeration
390 rates decreased with dilution of FLG suspensions from 3 mg/L to 0.1 mg/L, and the settling of FLG
391 was substantially slower at concentrations lower than 0.1 mg/L. Although cations induced fast
392 agglomeration when the IS approached 10 mmol/L NaCl, the presence of NOM effectively improved
393 the stability of FLG by electrostatic and steric interactions. Long-term stability studies suggest that
394 FLG agglomeration at low concentrations is expected in freshwater, but slow sedimentation may result
395 in continued FLG exposure to pelagic organisms. FLG entering seawater will be removed from the
396 water column at a rapid rate, and marine benthos may be at higher risk of exposure than aquatic
397 organisms. In addition, more attention should be paid to evaluating the environmental risk of small
398 FLG particles in consideration of their persistence at low concentrations and their high
399 bioaccumulation behaviors. The results from this study will aid in the choice of test media for aquatic
400 toxicity testing because exposing the organisms to a constant nanomaterial concentration by
401 minimizing agglomeration and sedimentation is typically a goal of these tests.

402

403 **Acknowledgments**

404 We acknowledge the financial support from the National Natural Science Foundation of China

405 (21377049, 21237001, and 21607072) and a Foundation for the Author of National Excellent Doctoral
406 Dissertation of PR China (201355). Certain commercial equipment, instruments and materials are
407 identified to specify experimental procedures as completely as possible. In no case does such
408 identification imply a recommendation or endorsement by the National Institute of Standards and
409 Technology nor does it imply that any of the materials, instruments or equipment identified are
410 necessarily the best available for the purpose.

411

412 **Appendix A. Supplementary data**

413 Additional details of experimental methods and results as well as other supporting tables and
414 figures.

415

416 **References**

- 417 Akkanen, J., Penttinen, S., Haitzer, M., Kukkonen, J.V.K., 2001. Bioavailability of atrazine, pyrene
418 and benzo[a]pyrene in European river waters. *Chemosphere* 45, 453-462.
- 419 Anderson, R., Barron, A.R., 2005. Reaction of hydroxyfullerene with metal salts: A route to
420 remediation and immobilization. *J. Am. Chem. Soc.* 127, 10458-10459.
- 421 Batley, G.E., Kirby, J.K., McLaughlin, M.J., 2012. Fate and risks of nanomaterials in aquatic and
422 terrestrial environments. *Acc. Chem. Res.* 46, 854-862.
- 423 Bouchard, D., Ma, X., Isaacson, C., 2009. Colloidal properties of aqueous fullerenes: Isoelectric points
424 and aggregation kinetics of C₆₀ and C₆₀ derivatives. *Environ. Sci. Technol.* 43, 6597-6603.
- 425 Bouchard, D., Zhang, W., Powell, T., Rattanadompol, U.s., 2012. Aggregation kinetics and transport
426 of single-walled carbon nanotubes at low surfactant concentrations. *Environ. Sci. Technol.* 46,
427 4458-4465.
- 428 Brown, L., Lochocki, E.B., Avila, J., Kim, C.-J., Ogawa, Y., Havener, R.W., Kim, D.-K., Monkman,
429 E.J., Shai, D.E., Wei, H.I., Levendorf, M.P., Asensio, M., Shen, K.M., Park, J., 2014.
430 Polycrystalline graphene with single crystalline electronic structure. *Nano Lett.* 14, 5706-5711.
- 431 Brunelli, A., Pojana, G., Callegaro, S., Marcomini, A., 2013. Agglomeration and sedimentation of
432 titanium dioxide nanoparticles (nTiO₂) in synthetic and real waters. *J. Nanopart. Res.* 15, 1-10.
- 433 Bussy, C., Ali-Boucetta, H., Kostarelos, K., 2013. Safety considerations for graphene: Lessons learnt
434 from carbon nanotubes. *Acc. Chem. Res.* 46, 692-701.
- 435 Chen, K.L., Elimelech, M., 2006. Aggregation and deposition kinetics of fullerene (C₆₀) nanoparticles.
436 *Langmuir* 22, 10994-11001.
- 437 Chen, K.L., Elimelech, M., 2008. Interaction of fullerene (C₆₀) nanoparticles with humic acid and
438 alginate coated silica surfaces: Measurements, mechanisms, and environmental implications.
439 *Environ. Sci. Technol.* 42, 7607-7614.
- 440 Chen, K.L., Elimelech, M., 2009. Relating colloidal stability of fullerene (C₆₀) nanoparticles to

441 nanoparticle charge and electrokinetic properties. *Environ. Sci. Technol.* 43, 7270-7276.

442 Chen, K.L., Mylon, S.E., Elimelech, M., 2006. Aggregation kinetics of alginate-coated hematite
443 nanoparticles in monovalent and divalent electrolytes. *Environ. Sci. Technol.* 40, 1516-1523.

444 Cho, E.C., Zhang, Q., Xia, Y., 2011. The effect of sedimentation and diffusion on cellular uptake of
445 gold nanoparticles. *Nat. Nanotechnol.* 6, 385-391.

446 Chowdhury, I., Duch, M.C., Mansukhani, N.D., Hersam, M.C., Bouchard, D., 2013. Colloidal
447 properties and stability of graphene oxide nanomaterials in the aquatic environment. *Environ. Sci.*
448 *Technol.* 47, 6288-6296.

449 Chowdhury, I., Mansukhani, N.D., Guiney, L.M., Hersam, M.C., Bouchard, D., 2015. Aggregation
450 and stability of reduced graphene oxide: Complex roles of divalent cations, pH, and natural
451 organic matter. *Environ. Sci. Technol.* 49, 10886-10893.

452 Deng, D., Pan, X., Yu, L., Cui, Y., Jiang, Y., Qi, J., Li, W., Fu, Q., Ma, X., Xue, Q., Sun, G., Bao, X.,
453 2011. Toward N-doped graphene via solvothermal synthesis. *Chem. Mater.* 23, 1188-1193.

454 Duch, M.C., Budinger, G.R.S., Liang, Y.T., Soberanes, S., Urich, D., Chiarella, S.E., Campochiaro,
455 L.A., Gonzalez, A., Chandel, N.S., Hersam, M.C., Mutlu, G.M., 2011. Minimizing oxidation and
456 stable nanoscale dispersion improves the biocompatibility of graphene in the lung. *Nano Lett.* 11,
457 5201-5207.

458 Eda, G., Fanchini, G., Chhowalla, M., 2008. Large-area ultrathin films of reduced graphene oxide as
459 a transparent and flexible electronic material. *Nat. Nanotechnol.* 3, 270-274.

460 Elimelech, M.G., J.; Jia, X.; Williams, R. A., 1995. Particle deposition and aggregation: Measurement,
461 modelling and simulation, Oxford, U.K.

462 Feng, Y., Lu, K., Mao, L., Guo, X., Gao, S., Petersen, E.J., 2015. Degradation of ¹⁴C-labeled few layer
463 graphene via Fenton reaction: Reaction rates, characterization of reaction products, and potential
464 ecological effects. *Water Res.* 84, 49-57.

465 Geim, A.K., 2009. Graphene: Status and prospects. *Science* 324, 1530-1534.

466 Gregory, J., 1981. Approximate expressions for retarded van der waals interaction. *J. Colloid Interface*
467 *Sci.* 83, 138-145.

468 Guo, X., Dong, S., Petersen, E.J., Gao, S., Huang, Q., Mao, L., 2013. Biological uptake and depuration
469 of radio-labeled graphene by *Daphnia magna*. *Environ. Sci. Technol.* 47, 12524-12531.

470 Hanus, L.H., Hartzler, R.U., Wagner, N.J., 2001. Electrolyte-induced aggregation of acrylic latex. 1.
471 Dilute particle concentrations. *Langmuir* 17, 3136-3147.

472 Holthoff, H., Egelhaaf, S.U., Borkovec, M., Schurtenberger, P., Sticher, H., 1996. Coagulation rate
473 measurements of colloidal particles by simultaneous static and dynamic light scattering.
474 *Langmuir* 12, 5541-5549.

475 Hsu, J.P., Liu, B.T., 1998. Critical coagulation concentration of a colloidal suspension at high particle
476 concentrations. *J. Phys. Chem. B* 102, 334-337.

477 Hu, X., Mu, L., Kang, J., Lu, K., Zhou, R., Zhou, Q., 2014. Humic acid acts as a natural antidote of
478 graphene by regulating nanomaterial translocation and metabolic fluxes in vivo. *Environ. Sci.*
479 *Technol.* 48, 6919-6927.

480 Hu, X., Zhou, M., Zhou, Q., 2015. Ambient water and visible-light irradiation drive changes in
481 graphene morphology, structure, surface chemistry, aggregation, and toxicity. *Environ. Sci.*
482 *Technol.* 49, 3410-3418.

483 Huang, G., Guo, H., Zhao, J., Liu, Y., Xing, B., 2016. Effect of co-existing kaolinite and goethite on
484 the aggregation of graphene oxide in the aquatic environment. *Water Res.* 102, 313-320.

485 Kaszuba, M., Corbett, J., Watson, F.M., Jones, A., 2010. High-concentration zeta potential
486 measurements using light-scattering techniques. *Philos. transact. A. Math. Phys. Eng. Sci.* 368,
487 4439-4451.

488 Konkana, B., Vasudevan, S., 2012. Understanding aqueous dispersibility of graphene oxide and
489 reduced graphene oxide through pKa measurements. *J. Phys. Chem. Lett.* 3, 867-872.

490 Kwon, D., Nho, H.W., Yoon, T.H., 2015. Transmission electron microscopy and scanning transmission
491 X-ray microscopy studies on the bioaccumulation and tissue level absorption of TiO₂
492 nanoparticles in *Daphnia magna*. *J. Nanosci. Nanotechnol.* 15, 4229-4238.

493 Lowry, G.V., Gregory, K.B., Apte, S.C., Lead, J.R., 2012. Transformations of nanomaterials in the
494 environment. *Environ. Sci. Technol.* 46, 6893-6899.

495 Lu, K., Huang, Q., Wang, P., Mao, L., 2015. Physicochemical changes of few-layer graphene in
496 peroxidase-catalyzed reactions: Characterization and potential ecological effects. *Environ. Sci.*
497 *Technol.* 49, 8558-8565.

498 Ma, J., Liu, R., Wang, X., Liu, Q., Chen, Y., Valle, R.P., Zuo, Y.Y., Xia, T., Liu, S., 2015. Crucial role
499 of lateral size for graphene oxide in activating macrophages and stimulating pro-inflammatory
500 responses in cells and animals. *ACS Nano* 9, 10498-10515.

501 Mao, L., Hu, M., Pan, B., Xie, Y., Petersen, E.J., 2016. Biodistribution and toxicity of radio-labeled
502 few layer graphene in mice after intratracheal instillation. *Part. Fibre Toxicol.* 13, 1-12.

503 Markus, A.A., Parsons, J.R., Roex, E.W.M., de Voogt, P., Laane, R.W.P.M., 2015. Modeling
504 aggregation and sedimentation of nanoparticles in the aquatic environment. *Sci. Total Environ.*
505 506-507, 323-329.

506 Maurer-Jones, M.A., Gunsolus, I.L., Murphy, C.J., Haynes, C.L., 2013. Toxicity of engineered
507 nanoparticles in the environment. *Anal. Chem.* 85, 3036-3049.

508 Medrzycka, K.B., 1991. The effect of particle concentration on zeta potential in extremely dilute
509 solutions. *Colloid Polym. Sci.* 269, 85-90.

510 Mu, Q., Su, G., Li, L., Gilbertson, B.O., Yu, L.H., Zhang, Q., Sun, Y.-P., Yan, B., 2012. Size-dependent
511 cell uptake of protein-coated graphene oxide nanosheets. *ACS Appl. Mater. Inter.* 4, 2259-2266.

512 Novoselov, K.S., Falko, V.I., Colombo, L., Gellert, P.R., Schwab, M.G., Kim, K., 2012. A roadmap
513 for graphene. *Nature* 490, 192-200.

514 Novoselov, K.S., Geim, A.K., Morozov, S.V., Jiang, D., Zhang, Y., Dubonos, S.V., Grigorieva, I.V.,
515 Firsov, A.A., 2004. Electric field effect in atomically thin carbon films. *Science* 306, 666-669.

516 OECD, 2013. OECD Guidelines for the testing of Chemicals, 236 "Fish embryo acute toxicity (FET)
517 test".

518 Orlova, V.V., van den Hil, F.E., Petrus-Reurer, S., Drabsch, Y., ten Dijke, P., Mummery, C.L., 2014.
519 Generation, expansion and functional analysis of endothelial cells and pericytes derived from
520 human pluripotent stem cells. *Nature Protoc.* 9, 1514-1531.

521 Pakarinen, K., Petersen, E.J., Alvila, L., Waissi-Leinonen, G.C., Akkanen, J., Leppänen, M.T.,
522 Kukkonen, J.V.K., 2013. A screening study on the fate of fullerenes (nC₆₀) and their toxic
523 implications in natural freshwaters. *Environ. Toxicol. Chem.* 32, 1224-1232.

524 Perreault, F., de Faria, A.F., Nejati, S., Elimelech, M., 2015. Antimicrobial properties of graphene
525 oxide nanosheets: Why size matters. *ACS Nano* 9, 7226-7236.

526 Petersen, E.J., Diamond, S.A., Kennedy, A.J., Goss, G.G., Ho, K., Lead, J., Hanna, S.K., Hartmann,
527 N.B., Hund-Rinke, K., Mader, B., Manier, N., Pandard, P., Salinas, E.R., Sayre, P., 2015.
528 Adapting OECD aquatic toxicity tests for use with manufactured nanomaterials: Key issues and
529 consensus recommendations. *Environ. Sci. Technol.* 49, 9532-9547.

530 Petersen, E.J., Henry, T.B., 2012. Methodological considerations for testing the ecotoxicity of carbon
531 nanotubes and fullerenes: Review. *Environ. Toxicol. Chem.* 31, 60-72.

532 Ramanathan, T., Abdala, A.A., Stankovich, S., Dikin, D.A., Herrera Alonso, M., Piner, R.D., Adamson,
533 D.H., Schniepp, H.C., Chen, X., Ruoff, R.S., Nguyen, S.T., Aksay, I.A., Prud'Homme, R.K.,
534 Brinson, L.C., 2008. Functionalized graphene sheets for polymer nanocomposites. *Nat.*

535 Nanotechnol. 3, 327-331.

536 Rawson, D.M., Zhang, T., Kalicharan, D., Jongebloed, W.L., 2000. Field emission scanning electron
537 microscopy and transmission electron microscopy studies of the chorion, plasma membrane and
538 syncytial layers of the gastrula-stage embryo of the zebrafish *Brachydanio rerio*: A consideration
539 of the structural and functional relationships with respect to cryoprotectant penetration. *Aquacult.*
540 *Res.* 31, 325-336.

541 Sano, M., Okamura, J., Shinkai, S., 2001. Colloidal nature of single-walled carbon nanotubes in
542 electrolyte solution: The Schulze–Hardy rule. *Langmuir* 17, 7172-7173.

543 Schedin, F., Geim, A.K., Morozov, S.V., Hill, E.W., Blake, P., Katsnelson, M.I., Novoselov, K.S., 2007.
544 Detection of individual gas molecules adsorbed on graphene. *Nat. Mater.* 6, 652-655.

545 Schinwald, A., Murphy, F.A., Jones, A., MacNee, W., Donaldson, K., 2012. Graphene-based
546 nanoplatelets: A new risk to the respiratory system as a consequence of their unusual aerodynamic
547 properties. *ACS Nano* 6, 736-746.

548 Seabra, A.B., Paula, A.J., de Lima, R., Alves, O.L., Durán, N., 2014. Nanotoxicity of graphene and
549 graphene oxide. *Chem. Res. Toxicol.* 27, 159-168.

550 Segal, M., 2009. Selling graphene by the ton. *Nat. Nanotechnol.* 4, 612-614.

551 Silva, T., Pokhrel, L.R., Dubey, B., Tolaymat, T.M., Maier, K.J., Liu, X., 2014. Particle size, surface
552 charge and concentration dependent ecotoxicity of three organo-coated silver nanoparticles:
553 Comparison between general linear model-predicted and observed toxicity. *Sci. Total Environ.*
554 468–469, 968-976.

555 Smith, B., Wepasnick, K., Schrote, K.E., Bertele, A.R., Ball, W.P., O’Melia, C., Fairbrother, D.H.,
556 2008. Colloidal properties of aqueous suspensions of acid-treated, multi-walled carbon nanotubes.
557 *Environ. Sci. Technol.* 43, 819-825.

558 Smith, B., Wepasnick, K., Schrote, K.E., Cho, H.H., Ball, W.P., Fairbrother, D.H., 2009. Influence of
559 surface oxides on the colloidal stability of multi-walled carbon nanotubes: A structure–property
560 relationship. *Langmuir* 25, 9767-9776.

561 Stankovich, S., Dikin, D.A., Dommett, G.H.B., Kohlhaas, K.M., Zimney, E.J., Stach, E.A., Piner, R.D.,
562 Nguyen, S.T., Ruoff, R.S., 2006. Graphene-based composite materials. *Nature* 442, 282-286.

563 Tezak, N., Matijevic, E., Schulz, K., 1951. Coagulation of hydrophobic sols in statu nascendi. II. Effect
564 of the concentration of the sol and of the stabilizing ion on the coagulation of silver chloride,
565 silver bromide, and silver iodide. *J. Phys. Colloid Chem.* 55, 1567-1576.

566 Wang, X., Zhi, L., Müllen, K., 2008. Transparent, conductive graphene electrodes for dye-sensitized
567 solar cells. *Nano Lett.* 8, 323-327.

568 Wu, L., Liu, L., Gao, B., Muñoz-Carpena, R., Zhang, M., Chen, H., Zhou, Z., Wang, H., 2013.
569 Aggregation kinetics of graphene oxides in aqueous solutions: Experiments, mechanisms, and
570 modeling. *Langmuir* 29, 15174-15181.

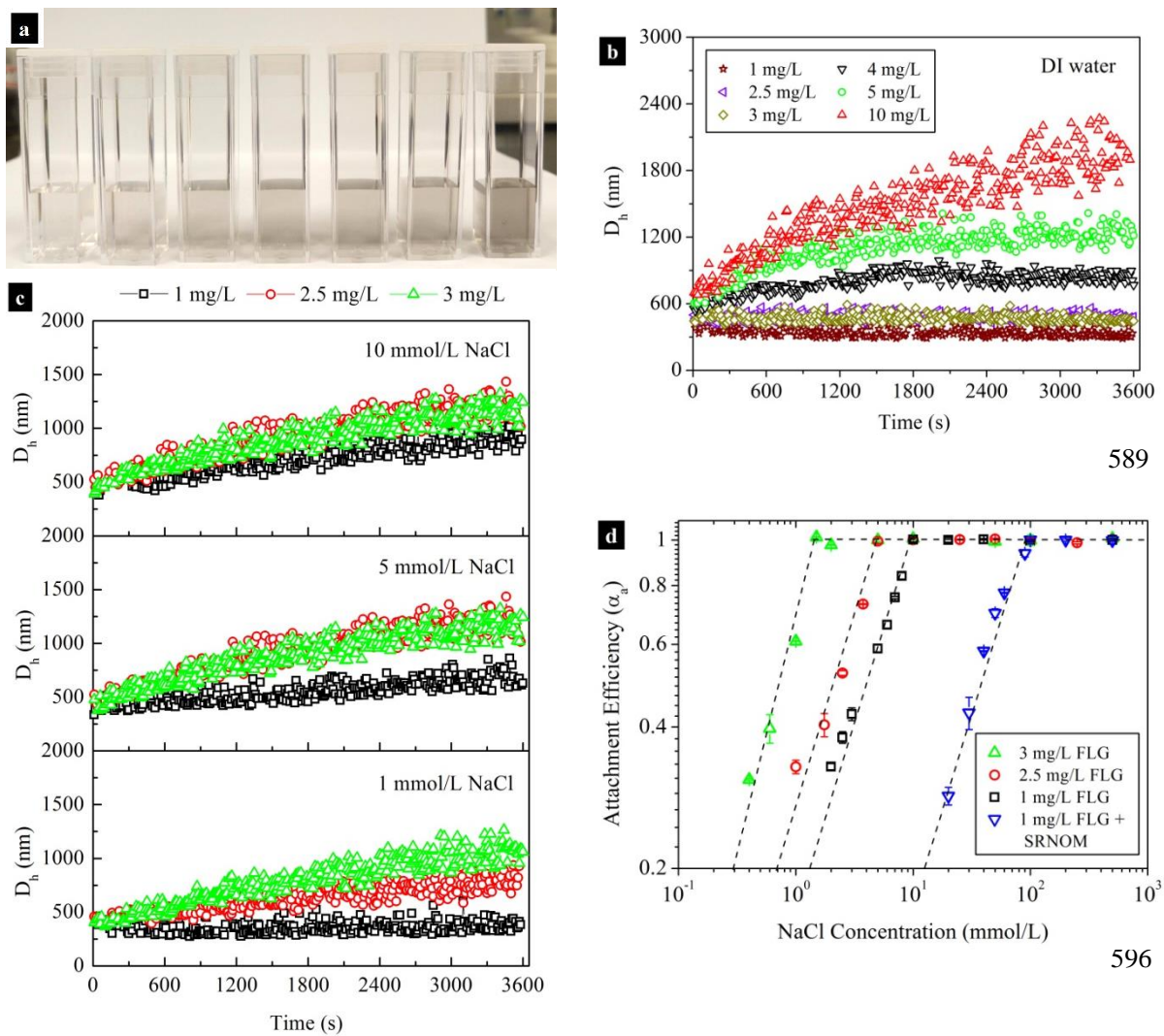
571 Yang, K., Wan, J., Zhang, S., Zhang, Y., Lee, S.-T., Liu, Z., 2011. In vivo pharmacokinetics, long-term
572 biodistribution, and toxicology of PEGylated graphene in mice. *ACS Nano* 5, 516-522.

573 Yang, K., Zhang, S., Zhang, G., Sun, X., Lee, S.-T., Liu, Z., 2010. Graphene in mice: Ultrahigh in vivo
574 tumor uptake and efficient photothermal therapy. *Nano Lett.* 10, 3318-3323.

575 Yi, P., Chen, K.L., 2011. Influence of surface oxidation on the aggregation and deposition kinetics of
576 multiwalled carbon nanotubes in monovalent and divalent electrolytes. *Langmuir* 27, 3588-3599.

577 Zhang, Y., Ali, S.F., Dervishi, E., Xu, Y., Li, Z., Casciano, D., Biris, A.S., 2010. Cytotoxicity effects
578 of graphene and single-wall carbon nanotubes in neural pheochromocytoma-derived PC12 cells.
579 *ACS Nano* 4, 3181-3186.

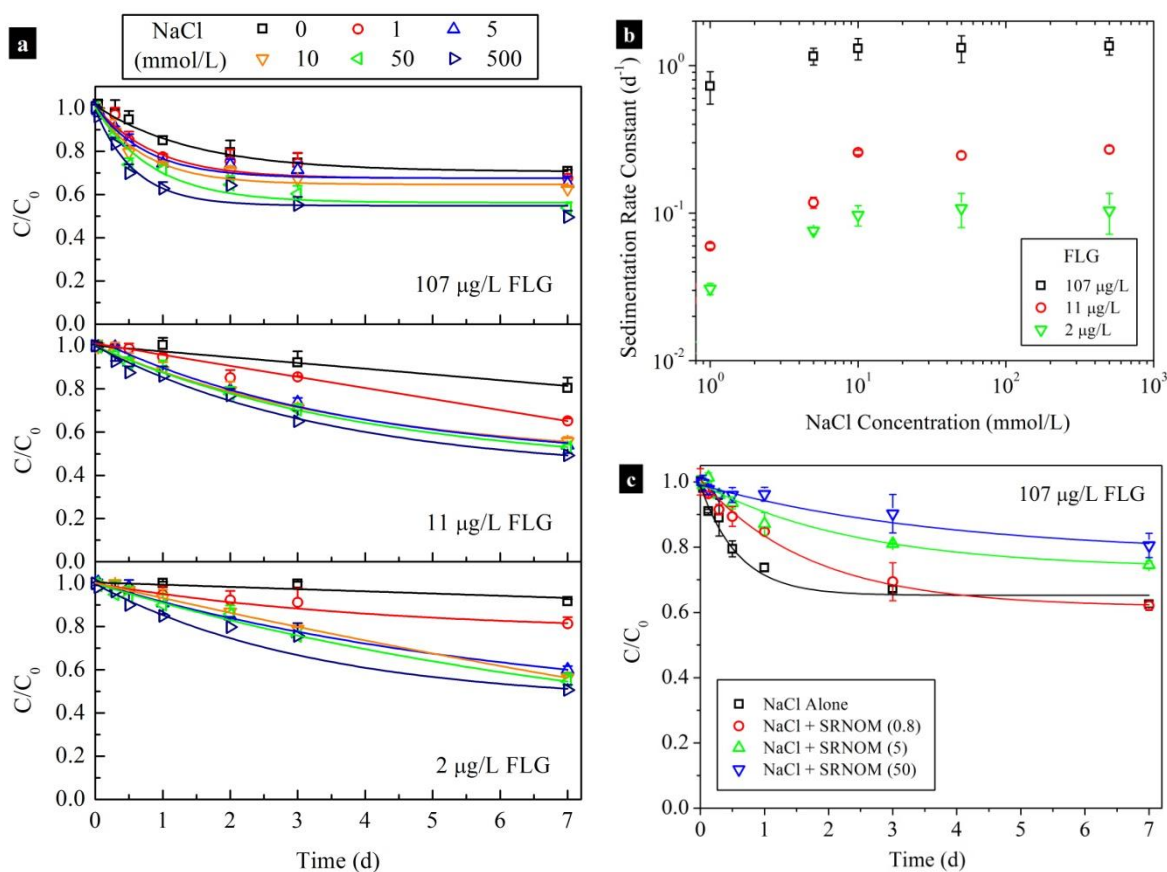
580 Zhao, C.M., Wang, W.X., 2012. Size-dependent uptake of silver nanoparticles in *Daphnia magna*.
581 *Environ. Sci. Technol.* 46, 11345-11351.



598 **Fig. 1.** (a) Photograph of cuvettes containing various concentrations of FLG dispersed in DI water.
 599 Agglomeration profiles of FLG in DI water (b) or NaCl solutions (c) at various FLG concentrations at
 600 pH 7.0. Attachment efficiencies (d) of FLG determined at different FLG concentrations as a function
 601 of NaCl concentration (pH 7.0) in the absence and presence of 0.57 mg TOC/L SRNOM; data points
 602 are mean and standard deviation values that calculated from triplicate samples.

603

604

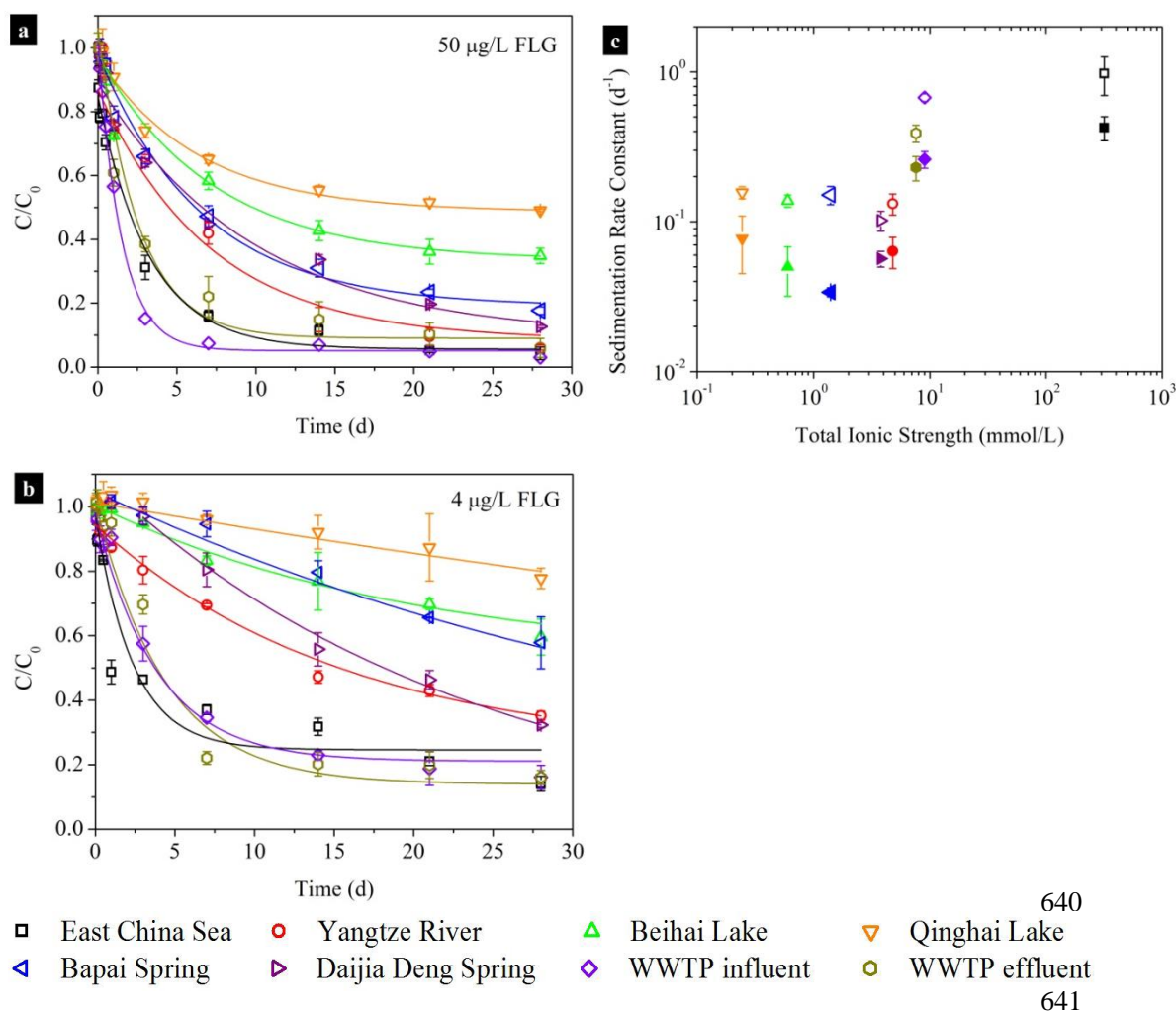


618 **Fig. 2.** (a) Normalized FLG concentration suspended in NaCl solution at three different initial
 619 concentrations (107 ± 3 , 10.7 ± 0.4 , and 1.980 ± 0.008) $\mu\text{g/L}$ ($n=3$; uncertainties indicate standard
 620 deviation values). Sedimentation rate constants (b) of FLG as a function of NaCl concentration at
 621 initial FLG concentrations of (107 ± 3 , 10.7 ± 0.4 , and 1.980 ± 0.008) $\mu\text{g/L}$ ($n=3$); data points are mean
 622 and standard error values that obtained from Table S5. (c) Stability of FLG in 10 mmol/L NaCl in the
 623 absence and presence of SRNOM. The C/C_0 values are mean and standard deviation values that
 624 calculated from triplicate samples.

625

626

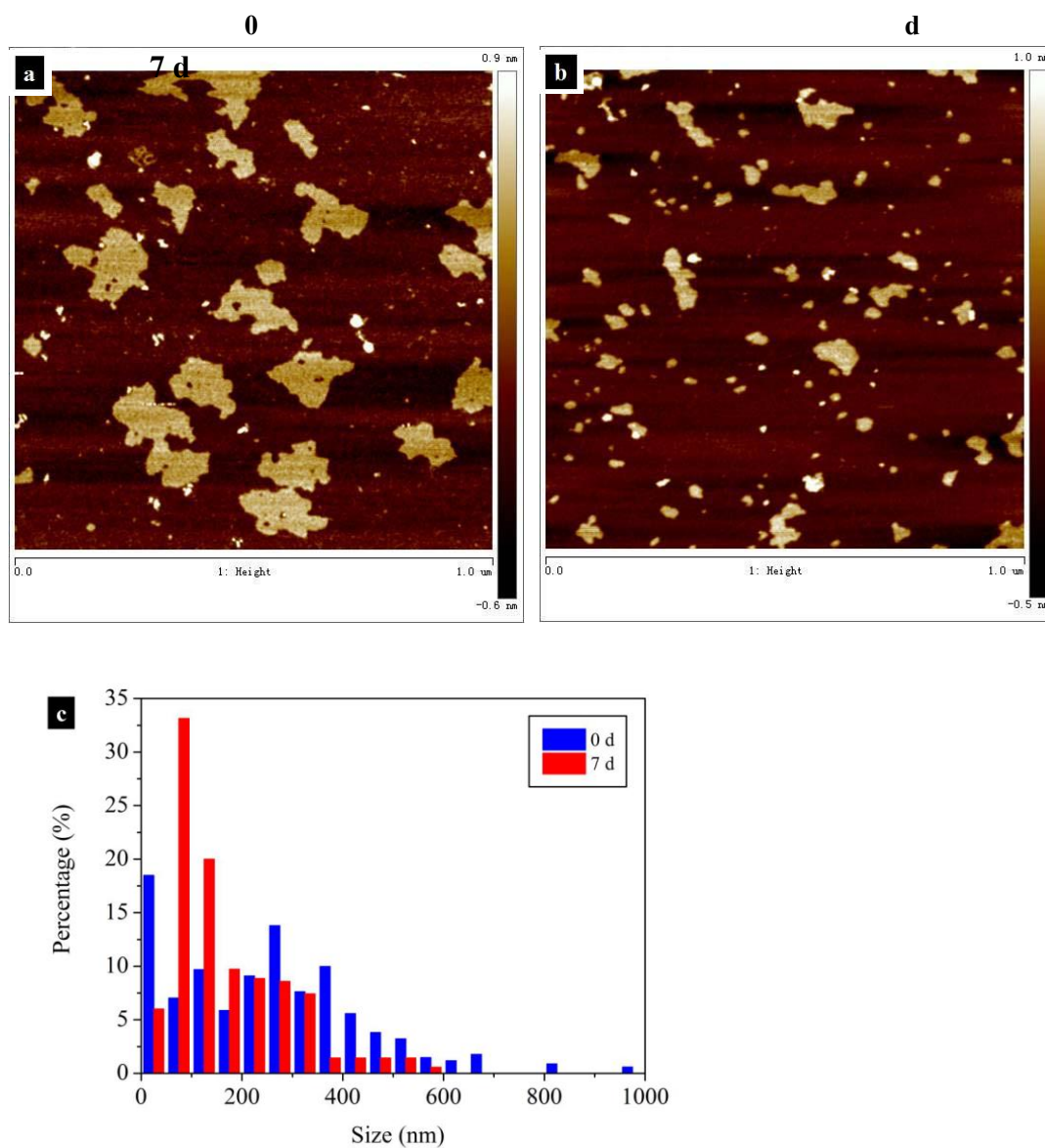
627



642 **Fig. 3.** Long-term stability of FLG in ambient waters and wastewater samples from a municipal
 643 wastewater treatment plant (WWTP). Normalized FLG concentrations in different types of water, the
 644 initial FLG concentration was 50 $\mu\text{g/L}$ ($50 \pm 2 \mu\text{g/L}$, $n=3$) (a) and 4 $\mu\text{g/L}$ ($3.90 \pm 0.03 \mu\text{g/L}$, $n=3$) (b),
 645 respectively. Data points are mean and standard deviation values that calculated from triplicate
 646 samples. Sedimentation rate constants (c) of FLG at initial concentrations of 50 $\mu\text{g/L}$ (open symbols)
 647 and 4 $\mu\text{g/L}$ (solid symbols) as a function of total ionic strength of the water samples. Data points are
 648 mean and standard error values that obtained from Table S7. Details for water sampling locations and
 649 water characteristics are provided in Table S1 and Table S6.

650

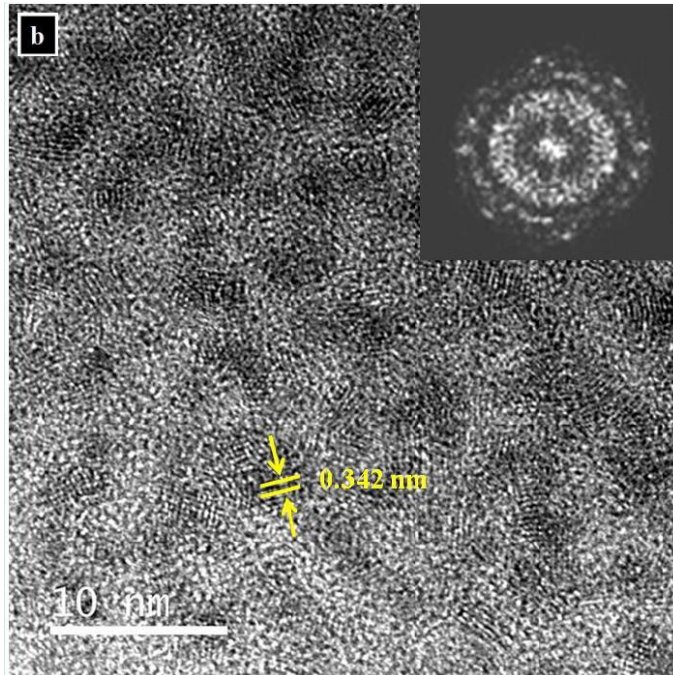
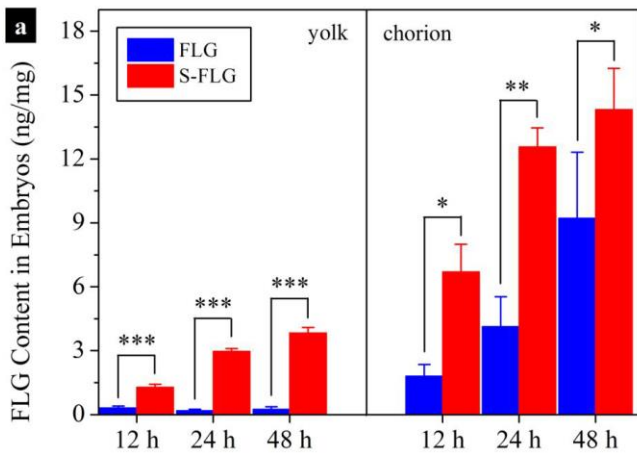
651



664

665 **Fig. 4.** Morphological characterization of FLG that suspended in 10 mmol/L NaCl solution before and
 666 after sedimentation for one week. The concentrations of FLG were 1097 ± 20 and 823 ± 28 $\mu\text{g/L}$ at 0
 667 d and 7 d, respectively ($n=3$; uncertainties indicate standard deviation values). Representative AFM
 668 images of FLG sampled at 0 d (a) and 7 d (b). (c) Histogram of FLG size distribution. The histograms
 669 were developed by counting 300 sheets for each FLG sample.

670



690 **Fig. 5.** (a) Effects of lateral size on uptake of FLG by zebrafish embryos and distribution of FLG in
 691 chorion and yolk. Zebrafish embryos were exposed to $(75 \pm 1) \mu\text{g/L}$ of FLG and small FLG (S-FLG)
 692 ($n=3$; uncertainties indicate standard deviation values). Data points are mean and standard deviation
 693 values that calculated from triplicate samples. Asterisks indicate statistical difference (*, $p<0.05$; **, $p<0.01$;
 694 ***, $p<0.001$) between treatments. (b) HRTEM images taken from ultra-thin section of the
 695 yolk that exposed to the S-FLG for 48 h; Inset: fourier transfer image of (b) indicates the crystalline
 696 structure of graphene.

697